Thermally tuneable optical and electrochemical properties of Au-Cu nanomosaic formed over the host titanium dimples

Wiktoria Lipińska, Katarzyna Grochowska, Jakub Karczewski, Jacek Ryl, Adam Cenian, Katarzyna Siuzdak

PII: S1385-8947(20)31801-5
DOI: https://doi.org/10.1016/j.cej.2020.125673
Reference: CEJ 125673

To appear in: *Chemical Engineering Journal*

Received Date: 20 March 2020
Revised Date: 21 May 2020
Accepted Date: 26 May 2020

Please cite this article as: W. Lipińska, K. Grochowska, J. Karczewski, J. Ryl, A. Cenian, K. Siuzdak, Thermally tuneable optical and electrochemical properties of Au-Cu nanomosaic formed over the host titanium dimples, *Chemical Engineering Journal* (2020), doi: https://doi.org/10.1016/j.cej.2020.125673

Thermally tuneable optical and electrochemical properties of Au-Cu nanomosaic formed over the host titanium dimples

Wiktoria Lipińska[1], Katarzyna Grochowska[1], Jakub Karczewski[2], Jacek Ryl[3], Adam Cenian[1] and Katarzyna Siuzdak[1]

[1]Centre for Plasma and Laser Engineering, The Szewalski Institute of Fluid-Flow Machinery Polish Academy of Sciences, Fiszera 14 St., 80-231 Gdańsk, Poland

[2]Faculty of Applied Physics and Mathematics, Gdańsk University of Technology, Narutowicza 11/12 St., 80-233 Gdańsk, Poland

[3]Faculty of Chemistry, Gdańsk University of Technology, Narutowicza 11/12 St., 80-233 Gdańsk, Poland

Abstract

Au-Cu nanostructures offer unique optical and catalytic properties unlike the monometallic ones resulting from the specific interaction. Among others, they have the ability to exhibit surface plasmon resonance, electrochemical activity towards the oxygen and hydrogen evolution reaction (OER, HER) as well as improved photoresponse in relation to monometalic but those properties depend highly on the substrate where bimetallic structures are immobilized.

In this work, bimetallic gold-copper mosaics over the conducting structured titanium substrate were fabricated via following steps: anodization of Ti foil, chemical etching of as-formed titania resulting in nanodimpled Ti substrate (TiND), sputtering of thin metal layer (Au, Cu) in various sequences, and finally thermal treatment in furnace at 450°C or 600°C. The morphology, optical and structural properties were investigated in details and it was shown that

both arrangements of metallic films and thermal conditions strongly affect the morphology and optical features. The XPS results confirmed the presence of gold-copper alloys and copper oxide species. Last but not least, the electrochemical activities were verified in 0.1 M NaOH using cyclic voltammetry and linear voltammetry measurements performed in dark and under visible light illumination. Among all investigated materials in both anodic and cathodic regimes bimetallic 5Au/5Cu sample annealed at 450°C exhibits the highest response towards OER and HER, respectively. This is further boosted by the light with λ>420 nm. Upon exposure to visible light, the current density for 5Au/5Cu and 5Cu/5Au electrodes reached 1.32 mA cm^{-2} and 1.26 mA cm^{-2}, respectively, while in the case of monometallic structures the current was below 10 µA cm^{-2}. Both optical and electrochemical behaviour indicate a strong synergistic effect arising within the bimetallic mosaic formed over the TiND.

Keywords

Au-Cu bimetallic nanostructures, broad band absorbance, oxygen evolution reaction, electrochemical activity, photoelectrochemical activity

Introduction

Nowadays, the possibilities of fabricating and modifying novel functional materials are widening, due to the rapid development of technology and easier access to the chemical compounds and advanced machines. Nevertheless, taking into account the total production cost, energy consumption as well as waste disposal, special interest is targeted on synthesis methods requiring simple equipment, lowering the usage of precious metals as well as avoiding additional purification steps. Due to the devastation of the environment, both the production of the new nanostructures and their further utilization towards energy conversion and storage should be at the centre of scientists' interest. Realizing the danger of resource depletion, the

global warming effect, air pollution and water contamination, the efforts of materials science should be focused on green synthesis methods and efficient usage of resources. Following that, the structures based on metal nanoparticles (NPs) not only reduce material consumption but due to change of their size from the macro to the nano scale they also reveal the unique properties, such as developed surface area, high electric capacitance and conductivity or light absorption in the visible range[1]. Among others, gold nanostructures have been widely explored and successfully applied in organic photovoltaic cells, photocatalysis and electrochemical sensors[2,3,4]. However, the depletion and rising price of precious metals as well as the safety concerns relating to the use of auric acid[5] force us to find some promising alternative to the monometallic gold structures as well as towards wet chemistry methods. Taking into account those challenges, the reduction of gold consumption in favour of other transition metals, e.g. Ag, Cu, Ni[6,7,8] as well as the application of physical top-down technique[9] have been proposed as a more environmentally friendly approach.

Following that, the significant growth of interest in the bimetallic Au-Cu nanostructures exhibiting unique optical and catalytical properties is not surprising[10,11,12]. Those extraordinary optical properties in most cases are related to the surface plasmon resonance (SPR) effect. The SPR is based on the excitation of plasmons, i.e. collective oscillations of free electrons, by light resulting in the enhancement of electromagnetic field arising in the nearest vicinity of the nanoparticles. It should be noted here that optical properties of NPs do not depend only on their chemical composition; but also their dimensions and shape, as well as the surrounding medium, are of high importance. Customarily, gold nanoparticles with dimensions from 5 to 50 nm exhibit absorption peak between 520-530 nm[13]. On the other hand, Cu nanoparticles with diameter of 20 nm show the maximum absorption peak at 580 nm[13]. However, when one combines gold and copper together, it is possible to achieve broadband absorption in the visible range[1] and its tuning within the several tens of nm is achievable. For the NPs of 10 nm in

diameter surrounded by a medium of 1.4 refractive index, the SPR maxima for Au, Au_3Cu, AuCu, $AuCu_3$, Cu were located at 532 nm, 538 nm, 561 nm, 567 nm, 578 nm, respectively[14]. Apart from the optical features, Au-Cu NPs are characterized by attractive catalytical properties especially towards the electrocatalytic reduction of CO_2[15] and selective alcohol oxidation[11]. Moreover, reports on the Au/Cu_2O porous heterostructures indicate their higher photoresponse comparing to the pure Cu_2O structure[16]. The oxygen evolution reaction (OER), as well as hydrogen evolution reaction (HER) running efficiently at Au-Cu bimetallic structures, were confirmed[17]. Therefore, the Au-Cu NPs can be successfully used in processes dealing with the environmental pollution present in liquid media.

It should be also noted, that the synthesis of Au-Cu bimetallic material not only takes advantage of the lower price of Cu cf Au but also take advantage of the high stability of gold[1]. In such materials, the improved properties of bimetallic structures occur due to the synergistic effect between both metals and this interaction depends on the structure inside the particular Au-Cu NP. The bimetallic nanoparticles can be classified into alloy/intermetallic or core-shell/layer-by-layer structures. In the case of Au-Cu, one can distinguish three different structures of specific stoichiometry such as $AuCu_3$, AuCu and Au_3Cu depending on the composition of individual elements[18]. Analyzing the Au-Cu phase diagram, it can be seen that at 410°C (1:1 atomic ratio) there is an order-disorder transformation[19], which is related to ordered intermetallic structures or disordered alloy creation. It was found that control of the ordering degree of Au-Cu nanoparticles significantly impacts the electrocatalytic activity[20]. The ordered structures exhibit high catalytic properties towards CO_2 to CO reduction, however the disordered ones enable enhanced hydrogen evolution[20]. Thus, it is very important to control precisely the synthesis procedure of the bimetallic nanoparticles as well as to reveal the electrochemical activity that could be further utilized in the reactions important from the environmental point of view.

In this paper, the synthesis of Au-Cu bimetallic nanomosaics over the textured Ti substrate as well as their morphology, structural, optical, electrochemical and photoelectrochemical characterization are studied. The titanium platform was fabricated via the electrochemical anodization process of Ti foil followed by the selective chemical etching of as formed titania nanotubes. As a result of that process, the ordered titanium nanodimples (TiND) were obtained acting further as host wells. Afterwards, that platform was covered by thin metal layers of Au and Cu in various sequences using the magnetron sputtering technique. In the next stage, the rapid thermal annealing at 450°C or 600°C was carried out. For reference, the same procedure was applied to the pristine TiND and TiND with deposited monometallic Cu and Au films. The morphology of materials was investigated by scanning electron microscopy (SEM) and atomic force microscopy (AFM). Fabricated samples were also characterized by X-ray photoelectron spectroscopy (XPS) for the determination of the oxidation states of atoms that form nanomosaics. On the basis of reflectance spectra recorded by UV-vis spectrophotometer the optical properties of nanostructures were analysed. Finally, the electrochemical and photoelectrochemical activities for the series of obtained structures were characterized both in dark and when the electrode was exposed to visible light. The linear voltammetry (LV) and cyclic voltammetry (CV) measurements in 0.1 M NaOH were carried out and significant differences between formed materials were identified. As expected, temperature strongly affects the morphology and properties of the resulting material. Finally, it has been experimentally proven that the synergistic effect between the Au and Cu can be achieved via simple thermal treatment of sputtered gold and copper films.

Experimental

Au-Cu electrode fabrication

Titanium foil (99.7%, Strem), acetone (Protolab), ethanol (96%, Chempur), ammonium fluoride (98%, Chempur), ethylene glycol (99%, Protolab) and oxalic acid dihydrate (99.5%, Sigma-Aldrich) were used for anodization and chemical etching processes of the as-anodized Ti foil. The pure targets of gold (99.99%, Quorum Technologies) and copper (99.99 %, Quorum Technologies) were used for thin metal layer deposition.

Firstly, the Ti foil was cut into 2×3 cm^2 rectangles and ultrasonically cleaned in acetone, ethanol and deionized water for 10 minutes in each medium. Immediately, the substrates were used for anodization. That process was conducted in the two-electrode system, where the Ti plate was used as an anode and Pt mesh as a cathode. Both electrodes were placed against each other 2 cm apart in the cylindrical glass cell. The reactor had a thermostatic jacket for the preservation of a constant temperature of 23°C during the whole process. The electrodes were immersed in the electrolyte composed of 0.27 M NH_4F dissolved in the mixture composed of 1% vol. deionized water and 99% vol. ethylene glycol. The anodization was carried out in two stages, the first one took 2 hours and the second 6 hours. At each stage the voltage of 40 V was applied between electrodes. After each anodization formed TiO_2 nanotubes were removed out of the Ti foil by selective chemical etching. This treatment involves the overnight immersion of samples in the 0.5% oxalic acid solution. This way, the titanium substrate covered uniformly by the nanodimples was obtained. Finally, the Ti nanotextured platform was rinsed with deionized water and dried. The obtained nanostructured titanium platform was covered by thin metal layers: 10 nm Au or 10 nm Cu or 5 nm Au and 5 nm Cu in both sequences, namely 5Au/5Cu and 5Cu/5Au using magnetron sputtering machine (Q150T S system, Quorum Technologies). Afterwards, samples were annealed at a temperature of 450°C or 600°C for 10 minutes. Thermal treatment was conducted in air atmosphere. The samples were placed onto the ceramic dish and then transferred to the muffle oven already heated to the established temperature. After processing they were taken out of the oven and left freely to cool down.

Samples characterization

Investigation of the electrodes morphology was performed using a field emission scanning electron microscope (FEI Quanta FEG250) equipped with an ET secondary detector and with the beam accelerating voltage kept at 10 kV. Additionally, the topography of TiND was studied by an atomic force microscope (AFM) (Nanosurf EasyScan 2). The reflectance spectra of nanostructures were measured by UV-vis spectrophotometer (Lambda 35, Perkin-Elmer) equipped with an accessory for reflectance spectra registration. The reflectance spectra registered with 60 nm/min speed in the wavelength range from 300 to 1000 nm were provided for the whole set of titanium, gold, copper and both types of gold-copper nanostructures.

The chemical nature of fabricated samples was revealed by X-ray photoelectron spectroscope (Escalab 250Xi, ThermoFisher Scientific) with a monochromatic AlKα source. Those measurements were carried out for the selected materials: 10Au, 10Cu, 5Au/5Cu and 5Cu/5Au annealed at 450°C, because of their prominent photoresponse as will be shown later on. The calibration for XPS spectra was based on the signal attributed to the pure Au metallic state (84.0 eV). The deconvolution of the XPS spectra was performed with Avantage v5.973 software (ThermoFischer Scientific).

The electrochemical and photoelectrochemical studies were conducted using the AutoLab PGStat 302N potentiostat-galvanostat, in the three-electrode arrangement placed in the cell containing a quartz window. The pristine TiND and modified TiND electrodes were used as the working electrode (WE) whereas Pt mesh was the counter electrode (CE) and Ag/AgCl/0.1M KCl was the reference electrode (RE). The cyclic voltammetry and linear voltammetry measurements were carried out in deaerated 0.1 M NaOH solution. The polarization curves were recorded from -0.8 V to +0.8 V vs. Ag/AgCl/0.1M KCl. For CV the scan rate was equal to 50 mV/s whereas for LV to 10 mV/s. In the case of photoelectrochemical

tests, the light source was a xenon lamp equipped with filters: AM 1.5 and UV cut-off (GG40, Schott). The irradiation intensity was established to be 100 mW/cm^2 using Si reference cell (Rera). The stability of electrochemical performance was verified by the multicyclic polarization accompanied with the recording of the linear voltammetry scan under visible light irradiation.

Results and discussion

Morphology

SEM images of the fabricated samples containing gold, copper and gold-copper metallic species onto titanium nanodimples annealed at 450°C and 600°C for 10 minutes are shown in Fig. 1. As it can be seen, the temperature strongly affects the morphology of materials obtained out of the sputtered thin layers and even the pristine TiND. As given in Fig. 1a and Fig. 1b the annealing at elevated temperature changes the dimensions of the dimples. The diameter of the bare titanium dimples for the sample annealed at 450°C was estimated to 75.5 ± 5.5 nm, while for the sample annealed at 600°C was equal to 54.08 ± 8.4 due to the variety of deformed substructure and changes in the grain size[21]. According to Chen et al., the recrystallization and the significant grain growth take place when the annealing is performed above 500°C. Moreover, other negative impact of higher temperature treatment is related with the hardness loss attributed to the decrease of dislocation density.

Regarding the case of pure gold, the thermal treatment at 450°C leads to the formation of a mosaic-like structure composed of Au NPs located in the host titanium dimples as presented in Fig. 1c which is in agreement with our previous works[22,23]. The electrode which has been annealed at the higher temperature of 600°C is shown in Fig. 1d and is characterized by a higher degree of disorder. As a result, in some areas of the sample bigger gold agglomerates can be found and therefore their size distribution is much wider comparing to the lower temperature conditions. Such phenomenon could be related to the changes of the TiND morphology itself.

SEM images provided in Fig. 1e and Fig. 1f show the copper species formed over the Ti and in both cases, in contrast to gold, no well separated NPs can be revealed. The only difference in material morphology in both temperature regimes is attributable to the grain size. The surface of 10Cu annealed at 450°C may be regarded as much smoother than 10Cu annealed at 600°C material where the sharp edges of individual grains can be observed. When SEM images of Au-Cu combinations are analysed, the morphology of the resulting structures can be regarded as a nano-mosaic composed of nanoparticles for the annealing performed under 600°C while lower temperature did not result in the creation of easily distinguished NPs on the FE SEM image. Nevertheless, when only 450°C was applied the characteristic dimples are still visible over the Ti substrate as presented in Fig. 1g and Fig. 1i. For the elevated temperature treatment, the whole substrate is almost uniformly covered by NPs but the dimpled nature of the substrate is not seen. This should be related to the changes in the geometrical dimensions of the TiNDs themselves thermally treated in two temperature regimes. The depth of TiND was calculated from AFM images (Fig. 2) and its average value for the material annealed at 450°C was 11.1 ± 2.3 nm (Fig. 2a), however for samples annealed at 600°C it was 7.3 ± 2.6 (Fig. 2b). Therefore, a higher temperature makes dimples shallower and in consequence the borders between dimples are less distinctive. For the complete characterization of structure also X-ray diffraction spectra were recorded and are shown (see Fig. S1) and described in the Supplementary Information file.

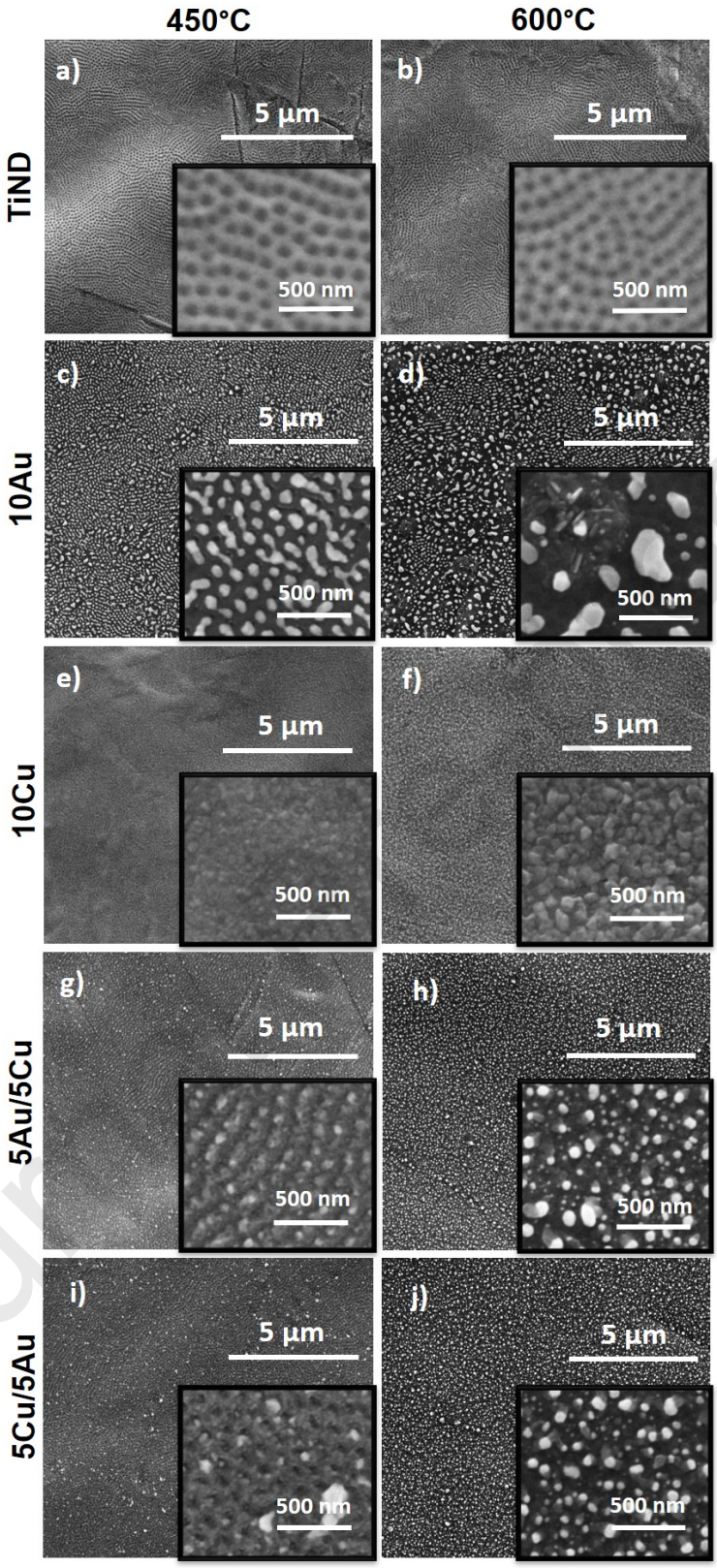

Fig.1. SEM images of the a) TiND (450°C), b) TiND (600°C), c) 10Au (450°C), d) 10Au (600°C), e) 10Cu (450°C), f) 10Cu (600°C), g) 5Au/5Cu (450°C), h) 5Au/5Cu (600°C), i)

5Cu/5Au (450°C), j) 5Cu/5Au (600°C). The temperature treatment was indicated in the round brackets.

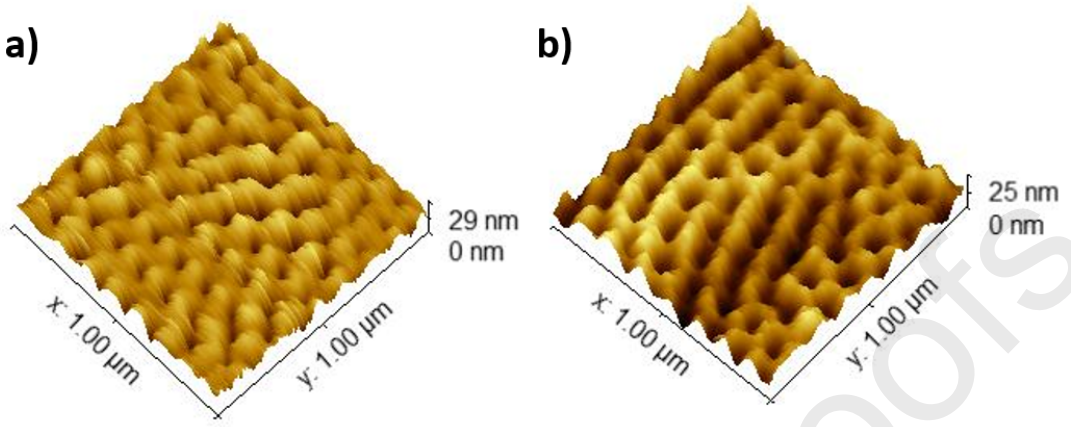

Fig. 2. Topographical AFM 3D image for TiND annealed at a) 450°C, b) 600°C.

Optical properties

The changes in the samples colour is clearly observed by the naked eye (Fig. 3) and since the samples are not transparent the reflectance spectra were recorded (see Fig. 4) to reveal unique optical properties. Regarding the provided digital photographs, one may observe variety of colours from metallic gold for 10Au annealed at 450°C to intense blue for 5Au/5Cu and 5Cu/5Au bimetallic mosaics formed at 600°C. For the bare substrate, namely TiND, the colour changes from light yellow to deep orange for 450°C and 600°C temperature conditions, respectively. As was reported by Skowroński et al.[24], similar observations regarding the colour impressions were noted for samples composed of titania film over Ti support where the gold tone is observed when the TiO_2 thickness reaches 11 nm and saturated blue in the case of almost 50 nm thick film. Those changes in material colours are in line with the modification of the reflectance shape. When 450°C was applied, the reflectance minimum for TiND is positioned at 330 nm whereas in the case of 600°C the reflectance band is broadened and the minimum is shifted to 450 nm. The coloration of the structure results from the interaction of the light and periodical lattice of NDs that allow to describe obtained material as a photonic crystal.

According to the morphology analysis, the change of the dimple dimension was observed and in consequence it modulates the position of the reflection band. Similar behaviour was reported by Umh et al. [25] and red shift was noted for Ti platforms composed of the uniformly distributed nanobowls fabricated at different anodization voltage.

When the thin metal films were deposited and then thermally treated, the shape of the reflectance spectra differs significantly due to the changes in the morphology as has been already described and of course depends on the type of deposited metal layer. The reflectance band minima for 10Au, 10Cu, 5Au/5Cu and 5Cu/5Au formed at 450°C are located at 360 nm, 580 nm, 470 nm and 480 nm, respectively (Fig. 4a). However, for 10Au, 10Cu, 5Au/5Cu and 5Cu/5Au annealed at 600°C, those minima are situated at ca. 510 nm, 890 nm, 900 nm and 910 nm (Fig. 4b). According to the literature, both when the modelling is applied[14] and for the experimental results[26] the SPR band for 10 nm gold nanoparticles is situated at ca. 520 nm while for copper at ca. 580 nm. Thus, only results for 10Au annealed at 600°C and Cu annealed at 450°C overlap those data. Moreover, because copper is an easily oxidized metal the comparison to Cu_2O nanoparticles is here justified. As was reported by Saad et al.[27] and Li et al.[28] the absorbance maximum situated at ca. 580 nm results from the exciton formation in Cu_2O. It should be also highlighted that the absorbance spectra significantly depend on the substrate used for NPs immobilization[29] and when the titania is used as a platform for Au nanospheres, the SPR absorbance maximum could be shifted from 400 nm for amorphous substrate up to 554 nm for anatase one. Therefore, we consider that in the case of the fabricated structures herein, especially 10Au (450°C) and 10Cu (600°C) the contribution to the reflectance originating from TiND is significant since for the substrate the absorbance maxima is located at 340 and 460 nm, respectively. Additionally, as was reported by Padikkaparambil et al.[30] decoration of the TiO_2 surface with gold led to a change in the intensity of the dioxide titanium absorption band. Two absorption maxima around 320 – 350 nm and 540 – 570 nm were correlated with different

amounts of Au deposited onto TiO_2. In our work, the amount of Au does not change, however, the amount of TiO_2 associated with the change of diameter and depth of nanodimples does, as well as Ti–Au surface interaction, caused by a higher degree of disorder.

Additionally, upon an increase of the annealing temperature the absorbance bands shift towards higher wavelength values by 150 and 310 nm for 10Au and 10Cu, respectively. According to Mohan et al.[31] the absorption band shift from 450 nm to 650 nm for CuO NPs were registered after annealing. However, we would like once again to emphasize the significance of the surface on which CuNPs as well as copper oxides are deposited and its influence on the SPR band location. According to Liu et al.[32] the maximum of absorbance band for CuNPs/FTO was positioned at 350 nm, while Pham et al.[33] showed that the maximum for Cu_2O/TNTs was found at c.a. 300 nm. Moreover, the usage of graphene oxide (GO) as a substrate results in minimum reflectance located at 750 nm for Cu_xO/GO configuration[34]. Those experimental findings support the explanation that the big shift of SPR band is determined by the type of platform used for further NPs deposition.

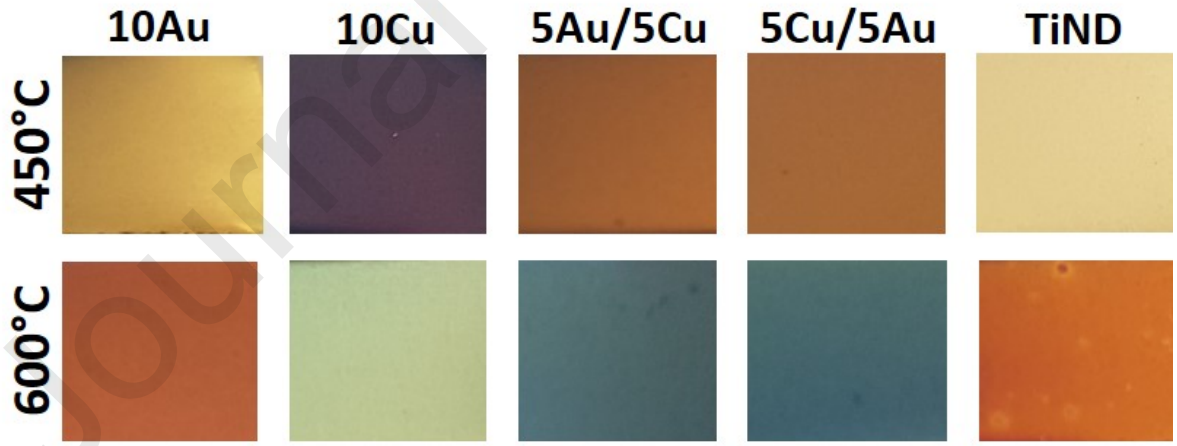

Fig. 3. Images of sample surfaces showing their colour changes due to different annealing temperature.

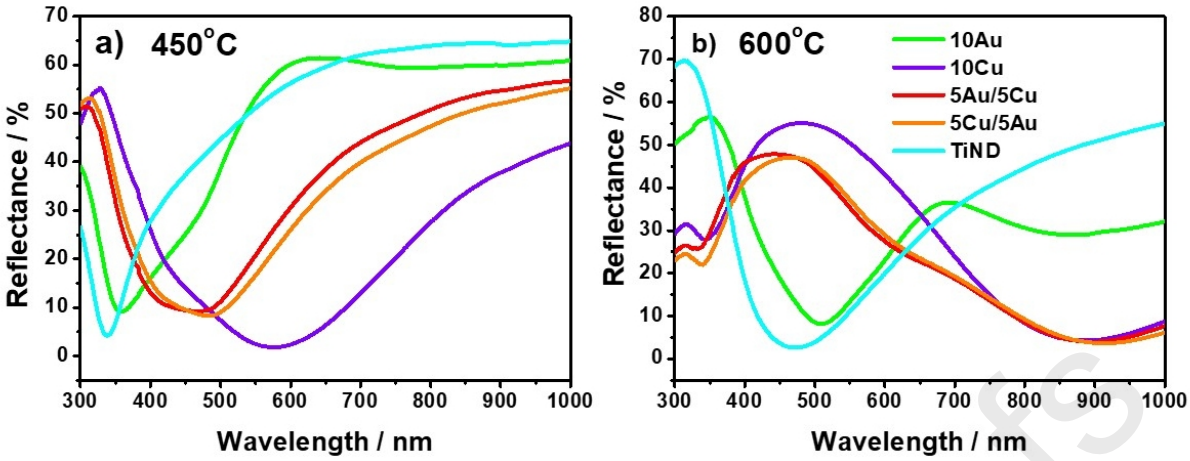

Fig. 4. Reflectance spectra of a) electrodes annealed at 450°C,

b) electrodes annealed at 600°C.

Regarding the bimetallic configurations, it should be highlighted that in both temperature regimes the shape of reflectance spectra for 5Au/5Cu and 5Cu/5Au nanomosaics almost overlaps and the local maxima and minima are positioned nearly at the same wavelengths for particular temperature case. Comparing the profiles of reflectance spectra for both Au-Cu arrangements the minima observed for the samples treated at 450°C correspond to the local maxima for the materials annealed at 600°C. For 5Au/5Cu and 5Cu/5Au samples the absorption bands are much wider compared to monometallic substrates but they are blue shifted regarding the band recorded for 10Cu treated at 450°C and overlap partially (above 750 nm) the spectra of 10Cu when the higher temperature annealing was carried out. It should be noted, that the absorption band for the bimetallic nanomosaic is red shifted compared to the monometallic gold layer treated at the same temperature regimes. This is in accordance with Sinha et al.[35] identifying the formation of single phase Au-Cu alloy as a responsible factor for such change.

Nevertheless, in our opinion the profiles of reflectance spectra for 5Au/5Cu and 5Cu/5Au electrodes manufactured in 450°C are strongly influenced by the TiND substrate as

well as the morphology of the Au-Cu structures. As it has been already mentioned during morphology analysis, the NPs formed at 600°C are much bigger and well distinguished than if only 450°C was applied. According to the literature, similar absorbance features were found for AuCu structures within the wide 600-1000 nm waverange[1]. The similar character for Au@Cu_2O reported by Liu et al.[36] and the significant red shift of the absorbance comparing to bare gold structure was explained by the introduction of Cu_2O to the system that is related with the increasing of the effective dielectric constant between the Au core and Cu_2O shell. Summarizing, both the annealing temperature, the composition of metallic layer and the nanotextured morphology of Ti substrate act here as key optical tuning factors.

Characterization of the chemical nature of samples

The chemical states of gold *Au4f* (Fig. 5a), copper *Cu2p* (Fig. 5b), titanium *Ti2p* (Fig. 5c) and oxygen *O1s* (Fig. 5d) were determined using X-ray photoelectron spectroscopy analysis. The detailed interpretation of all the recorded bands on the basis of the fitting procedure and peak deconvolution is presented below. The obtained results are summarized in Table 1. The high-resolution XPS spectrum for the *Au4f* appears as a peak doublet (Fig. 5a) and confirms the presence of metallic Au (84.0 eV) on the surface[37].

In the case of the high-resolution XPS spectrum for copper, the analysis revealed the diversity of *Cu2p* chemical states. Three separate chemical states were identified and considered for the spectral deconvolution, as shown in Fig. 5b. This element is present primarily as Cu(II) in two various forms: *Cu2p3/2* peak at 935.0 eV present in the energy range characteristic for $Cu(OH)_2$ and/or $CuCO_3$[38, 39], while CuO[40] was confirmed by the signal located at 933.5 eV. The third component arising at 932.8 eV[41] in the case of 10Cu sample was assigned to the metallic Cu with no contributions from other copper oxides[42,43]. Notably, regarding 5Au/5Cu as well as 5Cu/5Au alloys, the location of metallic Cu peak is negatively shifted by

0.4 and 0.5 eV, respectively[42]. The higher binding energy of Cu in the monometallic copper sample than in the bimetallic one is caused by electron transfer from Cu to Au which decreases the electron density within Cu[44]. The dominance of the various Cu(II) species within the analysed spectra is confirmed with satellite feature at approx. 940-945 eV, as well as Cu_{LMM} Auger spectrum, presented in Fig. S2 (Supplementary Information file). In the case of each investigated sample the spectra peaks are present at energy characteristic for Cu(II). This analysis confirms negligible presence or lack of Cu(I)[45].

In the case of titanium, its chemical states vary depending on the investigated material. For 10Au electrode the *Ti2p3/2* peak at 459.2 eV was characterized as TiO_2 which is present at the Au/Ti interface (Fig. 5c). However, for both the 5Au/5Cu and 5Cu/5Au mosaics, the *Ti2p3/2* peak appears negatively shifted by -0.8 eV and confirms the presence of Ti_2O_3[46] (Fig. 5c). Although, it is worth mentioning that the Ti share was minor compared to other components since it is covered by gold and copper metal species. Titanium was not detected for the 10Cu electrode, most likely due to the higher thickness of Cu because of the copper oxide formation acting as a TiND cover and the surface character of the XPS analysis.

Last but not least, the detailed analysis of the *O1s* spectrum (Fig. 5d) reveals a similar nature of oxygen species present in 10Cu, 5Au/5Cu and 5Cu/5Au electrodes. The strong peak at 529.6 eV was ascribed to the lattice oxygen in CuO[47]. Additionally, peaks located at 531.3 eV were linked to $Cu(OH)_2$ and surface adsorbed OH^-[39]. Unlike other analyses, the main component of *O1s* for 10 Au electrode (Fig. 5d) located at 530.5 eV was ascribed as lattice oxygen derived from titanium dioxide which is exposed to the oxygen rich atmosphere because of Au NPs creation. The second component was characterized as non-lattice oxygen in TiO_2 and hydroxyl species[48].

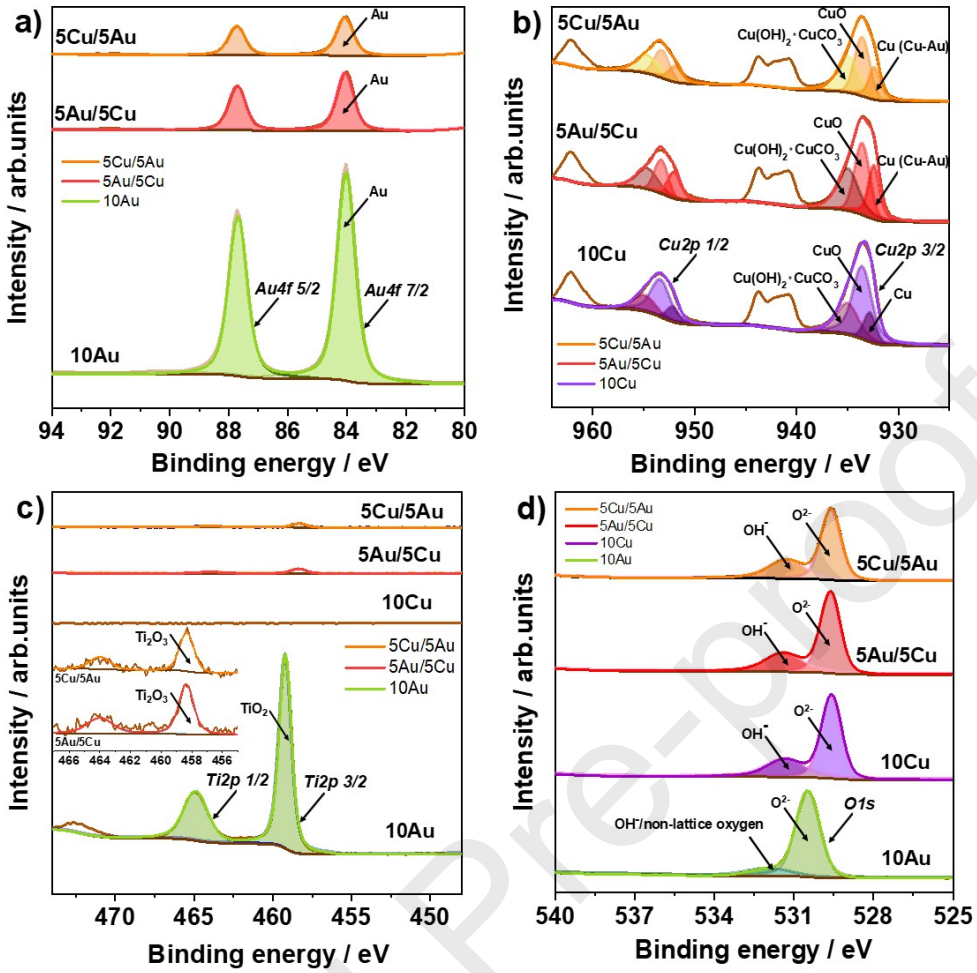

Fig.5 XPS high resolution spectra registered for 10Au, 10Cu, 5Au/5Cu and 5Cu/5Au samples annealed at 450°C: a) *Au4f*, b) *Cu2p*, c) *Ti2p* and d) *O1s*.

Table 1. The binding energies (BE) of 10Au, 10Cu, 5Au/5Cu and 5Cu/5Au samples annealed at 450°C used for XPS analysis.

Peak	Component	BE / eV	At. %	Component	BE / eV	At. %
	10Au			**10Cu**		
Au4f 7/2	Au	84.0	26.5	-	-	-
Cu2p 3/2	-	-	-	$Cu(OH)_2$ and	935.0	10.4

				$CuCO_3$		
Cu2p 3/2	-	-	-	CuO	933.5	21.6
Cu2p 3/2	-	-	-	Cu	932.8	4.8
Ti2p 3/2	TiO_2	459.2	21.5	-	-	-
O1s	non-lattice oxygen / OH^-	532.0	5.9	OH^-	531.3	19.9
O1s	O^{2-}	530.5	46.1	O^{2-}	529.6	43.3

	5Au/5Cu			**5Cu/5Au**		
Au4f 7/2	Au	84.1	7.1	Au	84.1	5.5
Cu2p 3/2	$Cu(OH)_2$ and $CuCO_3$	935.0	12.9	$Cu(OH)_2$ and $CuCO_3$	935.0	13.4
Cu2p 3/2	CuO	933.5	13.5	CuO	933.5	13.1
Cu2p 3/2	Cu (Cu-Au)	932.4	8.6	Cu (Cu-Au)	932.3	6.1
Ti2p 3/2	Ti_2O_3	458.4	0.7	Ti_2O_3	458.3	0.6
O1s	OH^-	531.4	19.1	OH^-	531.3	22.1
O1s	O^{2-}	529.6	38.1	O^{2-}	529.6	39.3

Electrochemical performance

The electrochemical activity of the bimetallic nanostructures was characterized using cyclic voltammetry measurements carried out in 0.1 M NaOH solution since gold and especially copper are then stable and do not dissolve, as has been already confirmed by other reports[49,50,51,52,53] and is in agreement with the Pourbaix diagram. The results obtained for bimetallic 5Au/5Cu and 5Cu/5Au structures are shown in Fig. 6 together with gold, copper and titanium nanodimpled samples thermally treated also at 450°C and 600°C. Comparing both

temperature regimes, the distinctive faradaic activities were observed when the materials were annealed at 450°C. The anodic peak observed at +0.3 V vs. Ag/AgCl/0.1M KCl for 10Au electrode corresponds to the formation of Au_2O_3, while at 0 V the reduction of gold oxides is recognized[50] (Fig. 6a). Regarding the 10Cu sample, the signal at -0.7 V is recognized as reduction of Cu(II) to Cu(I) while the other at c.a. +0.5 V is assigned to the oxidation of Cu(I) to Cu(II)[52]. Comparing the shapes of CV scans for materials annealed at 450°C, it should be noted that the unique pattern for the bimetallic electrodes was identified. The similar shape of voltamperograms in the potential range below +1.2 V vs. RHE were reported by Liu et al. [15] for Au-Cu films, however in our work much higher current densities were obtained at the anodic limit established here at +0.8 V. For both Au-Cu arrangements barely visible oxidation peaks are present at ca. -0.25 V and -0.05 V and more pronounced signals are observed at ca.-0.20 V, +0.05 V and +0.6 V corresponding to the reduction processes. An analogous set of signals was found for $Au_{50}Cu_{50}$ and $Au_{25}Cu_{75}$ samples and those oxidation peaks were ascribed by Liu et al.[15] to the formation of $Cu(OH)_2$ and then surface part of electrode material exhibits a duplex nature consisting of Cu_2O core and an outer $CuO/Cu(OH)_2$ layer. However, the oxidation processes are less distinctive comparing to the reduction ones indicating that presence of gold atoms inhibits those reactions. It was also confirmed by Passini et al.[54], concluding that such electrochemical activity of copper species present in the bimetallic structure occurs due to their stabilization by gold ones. On the reverse CV scan, the appearance of the reduction peak at -0.2 V could be interpreted as the change from metallic Cu to CuO[55] while at +0.05 V the reduction of gold oxides is demonstrated. In this work, the XPS results confirm the presence of CuO and $Cu(OH)_2$ species as well as the Cu-Au alloy. Therefore, the detailed analysis of XPS spectra supports the proposed interpretation of the signals arising on the CV curve recorded for the bimetallic electrode. Polarizing the working electrode towards anodic limit particularly at +0.7 V vs. Ag/AgCl/0.1M KCl, the OER is initiated. In this process the molecular oxygen is

generated via electrochemical oxidation of hydroxyl ions present in the basic solution: $4OH^- \rightarrow O_2 + 2H_2O + 4e^-$[56,57,58]. Such behaviour for other AuCu based structures was not reported in the literature and the electrochemical activity of such kind of electrodes is generally limited to the cathodic range and reduction processes as reported e.g. by Liu et al.[15], Chen et al.[59] and Wang et al.[60]. However, when TiND based materials were annealed at 600°C (see Fig. 6b) the recorded currents were much lower compared to those treated at 450°C and almost no faradaic peaks were noticed. Only in the case of pure gold layer some peak current at ca. 0 V ascribed to the reduction of gold oxides was observed[61]. It could be stated that such low electrochemical response results from the formation of highly resistive titania film identified as the rutile phase[62,63]. The significantly diminished activity of both mono- and bimetallic mosaic structures does not favour application of high temperature for the material processing despite morphology inspection indicating the ordered distribution of nanoparticles over the hosted TiNDs.

Additionally, according to Łukaszewski et al.[64], the real surface area of 5Au/5Cu material was estimated basing on the relation between the double layer charging current and the scan rate. As can be observed in Fig. S3, the slope value for 5Au/5Cu is much higher comparing to flat Au disc electrode. The polished Au disc electrode (diameter 2 mm, s = 0.0314 cm^2) acts here as the reference electrode material and since it is ideally flat - the geometric surface area is regarded as an electrochemically active one. Taking above into account and the values of slopes, the real surface area for 5Au/5Cu sample is 10.3 times higher comparing to the flat gold surface that positively impacts onto the overall electrochemical response.

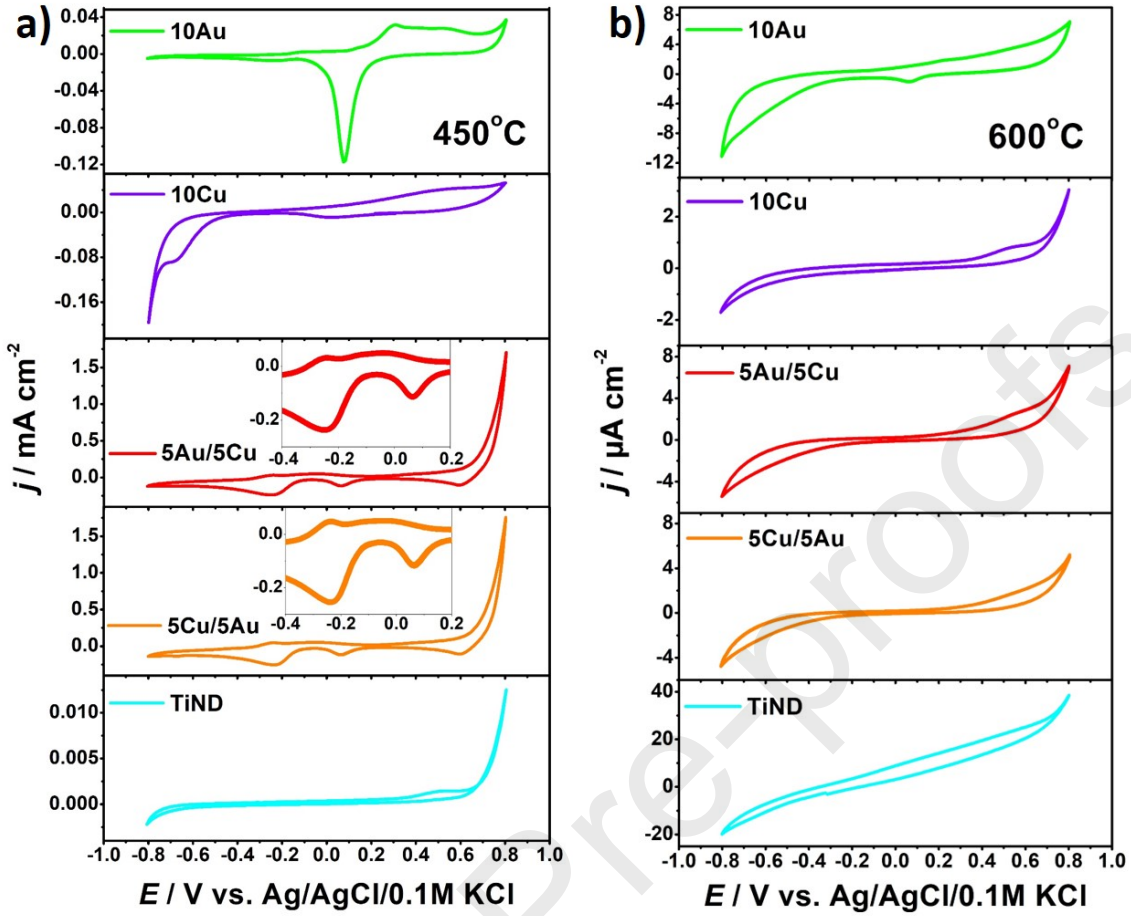

Fig. 6 Cyclic voltammetry curves registered in 0.1 M NaOH at the scan rate of 50 mV/s for samples annealed at a) 450°C and b) 600°C.

In order to study the photoactivity of the fabricated materials, the linear voltammetry measurements in dark and under visible illumination were carried out (Fig. 7). For the reference samples, namely TiND, 10Au and 10Cu one may observe very low photoresponse (several dozens of µA cm^{-2}) when the thermal annealing was applied at 450°C (Fig. 8). For the 10Au electrode (Fig. 8a) characteristic oxidation peak at +0.3 V arises at the same intensity in dark and under vis illumination while the photocurrent improvement starts above +0.6 V. However, the signal at +0.8 V might rather correspond to the oxidation of Au(110)[65] since any gas bubbles were not noticed at the electrode surface. Among other reference materials, for the 10Cu sample the activity towards HER below -0.4 V vs. Ag/AgCl/0.1M KCl was recognised which is typical

for copper-containing electrode materials[66]. Under illumination of 10Cu the overpotential increases (Fig. 8b). However, from -0.4 V to the anodic regime the sample exhibits photoanode character[67] but its activity towards effective OER is negligible. The small changes between current density in dark and under electrode illumination for TiND (Fig. 8c) are noticed due to the very thin TiO_2 layer. It is well known that photocurrent is strongly determined by the layer thickness[68,69], thus the presence of a very thin passivation layer of titania does not enable the efficient visible light absorption and photocurrent generation. In all cases of the monometallic materials, namely 10Au, 10Cu and TiND some increase of photocurrent exists but it is much lower than observed for 5Au/5Cu and 5Cu/5Au structures.

To track the difference value, the comparison of current densities recorded at +0.8 V vs. Ag/AgCl/0.1M KCl in dark and under irradiation were listed in Table 2. As could be observed, the 5Au/5Cu and 5Cu/5Au electrodes annealed at 450°C showed an impressive increase of both the electrochemical and photoelectrochemical activity in the anodic range above +0.6 V and at cathodic potential values below -0.6 V while at -0.18 V the boosted oxidation process can be distinguished (Fig. 7a).

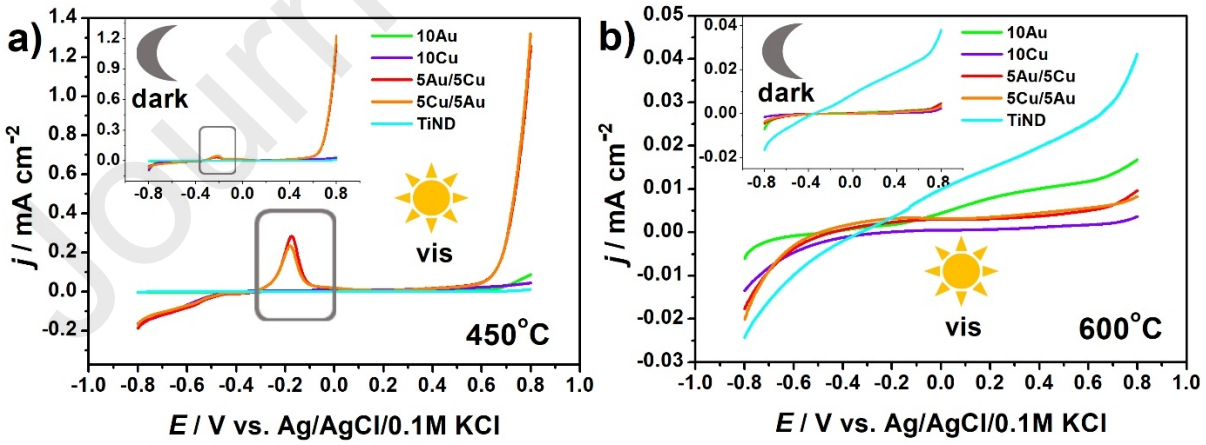

Fig. 7 Linear voltammetry curves registered in 0.1 M NaOH in dark and under visible illumination for samples annealed at a) 450°C and b) 600°C.

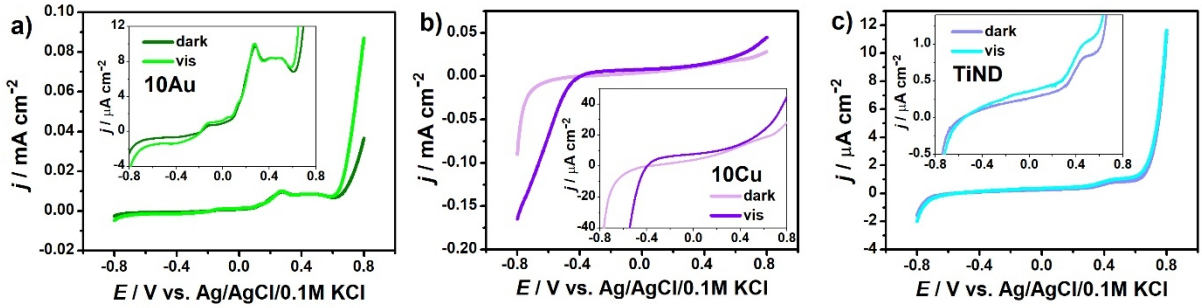

Fig. 8 Linear voltammetry curves registered in 0.1 M NaOH in dark and under visible illumination for samples annealed at 450°C: a) 10Au, b) 10Cu, c) TiND.

Taking into account the current density registered for 10Au (0.04 mA cm^{-2}), the combination of Au with Cu results in more than a 30 times enhancement (j = 1.23 mA cm^{-2} for 5Cu/5Au) proving the synergising effect arising from the integration between both metals. Following that, the impressive acceleration of the oxygen evolution reaction [58,17] takes place. According to other reports such a feature could be ascribed to the AuCu[17] and CuO[70] activity, as those species have been already confirmed by XPS studies. It should be also underlined that the highest anodic current enhancement was achieved for the 5Au/5Cu electrode and the difference between the current density recorded in dark and under exposure to visible light reaches 120 μA cm^{-2} whereas for the 5Cu/5Au configuration is lower and equals 90 μA cm^{-2}. This discrepancy results from the better separation of photogenerated charges onto the outer film composed of Cu species[71] in favour of 5Au/5Cu. We would like to highlight here that the formation of both Au/Cu nanomosaics requires only usage of a 5 nm thick copper layer and 5 nm thick gold layer in contrast to other bimetallic nanostructures where even microlong wires[72] or rods[73] are applied indicating high loading of precious metal but first of all usage of auric acid[74,75]. Moreover, according to Gong et al.[17] and Pawar et al.[70] the OER onset potential was much higher and equals even +1.7 V vs. RHE (ca. + 1.4 vs. Ag/AgCl/0.1M KCl) for AuCu branched nanostructures in 0.1 M KOH and +1.6 V vs. RHE (ca. +1.3 vs. Ag/AgCl/0.1M KCl) for CuO nanosheet in 1 M KOH.

Additionally, the oxidation process significantly enhanced by light took place at the potential of -0.18 V for 5Au/5Cu and 5Cu/5Au. Described electrode behaviour is repeatable as was verified by sequentially registered LV curves while any material detachment out of TiND support was not observed. In dark conditions the current density equals only 35 μA cm^{-2} and 50 μA cm^{-2} for 5Au/5Cu and 5Cu/5Au respectively, whereas almost 0.3 and 0.23 mA cm^{-2} was reached when the electrode was exposed to the radiation >420 nm. Similarly, such a distinctive oxidation peak was not observed for pure gold or copper reference materials as well as other gold-copper heterojunctions or metal-metal oxide combinations such as Au-Cu_2O core shell nanowires[71] as well as Au-CuO/n-Si[76], Au-$WzCuInS_2$/ITO[77], ZnO/Au/p-nCu_2O and ZnO/Au/nCu_2O[78] electrodes. However, according to Minggu et al.[79], this enhanced process is related to the Cu_2O oxidation ($Cu_2O + 2OH^- \rightarrow 2CuO + H_2O + 2e^-$) and the further current decrease may be related to the peeling of the copper oxide film. Following that, we regard that under irradiation the photogenerated holes are used in the oxidation process of Cu_2O while electrons are transferred via thin titania film towards the metallic substrate and in consequence a substantial current increase is recorded[80]. Since the absorbance spectra for 5Au/5Cu and 5Cu/5Au are very similar, the observed difference between those configurations may result from the various content of Au-Cu alloy species. As has been revealed by XPS inspection, the contribution of Au-Cu is in favour for arrangement where copper film was sputtered onto the gold. According to Sugano et al.[81], the synergistic effect within Au-Cu alloy positively impacts on the oxidation process while as was indicated by Liu et al.[82] copper affects intraband transition and ultimately promotes visible-light activity.

Table 2 The values of current density at +0.8 V vs. Ag/AgCl/0.1M KCl in dark and under visible light illumination for samples annealed at 450°C (Fig. 7).

sample	j (dark) / mA cm^{-2}	**sample**	j (vis)/ mA cm^{-2}

10 Au	0.04	10 Au	0.09
10 Cu	0.03	10 Cu	0.04
5Au/5Cu	**1.14**	5Au/5Cu	**1.26**
5Cu/5Au	**1.23**	5Cu/5Au	**1.32**
TiND	0.01	TiND	0.01

The other unique activity of Au/Cu systems was also recognized in the cathodic potential range. The values of current densities for particular materials treated at 450°C recorded in dark and under visible irradiation when the electrode was polarized at -0.8 V vs. Ag/AgCl/0.1M KCl were listed in Table 3 (also see Fig. 9). The cathodic current density for 5Au/5Cu increases from -50 to -190 μA cm^{-2} and for 5Cu/5Au changes from -60 to -170 μA cm^{-2} while for pure gold and bare titania never exceeded a few μA cm^{-2}. However, considering changes in the cathodic range for 10Cu sample similar behaviour to the bimetallic materials was observed and can be assigned to the Cu activity[83]. Proposed interpretation is in accordance with the explanation given for other copper containing systems e.g. ZnO/Cu_2O-CuO with embedded Cu(I) and Cu(II) oxides[84], TiO_2/CuO/Cu mesoporous nanofibers[85] and CuNPs on glass carbon or platinum electrodes[83] used for the efficient photocatalytic or catalytic HER evolution. We would like to underline that the achieved enhancement of current in both anodic and cathodic range when the electrode is exposed to visible light is also higher than for other materials of similar composition, e.g. for the Au-Cu alloy deposited onto titanium dioxide nanosheets where the difference between response recorded under light and in dark equals only ca. 10 μA cm^{-2} and the time dependent attenuation of photoactivity was registered[86]. A similar slight increment of photocurrent density was reported by Fu et al.[87] for ZnO@Au@Cu_2O nanotubes and by Xue et al.[88] for the Cu_2O cubes decorated with Au NPs.

It should be also underlined that the most active bimetallic structure 5Au/5Cu annealed at 450°C exhibits also high stability. The consecutive cyclic voltammetry scans almost overlap while the linear voltammetry curve recorded when the working electrode is exposed to the visible light (see Fig. S4) preserves its shape and corresponds to LV given in Fig. 7a. The continuation of multicyclic dynamic polarization of the material after LV scan also provides the same CV curves confirming resistance towards photocorosion.

Table 3 The values of current densities at -0.8 V vs. Ag/AgCl/0.1M KCl in dark and under visible light illumination for samples annealed at 450°C (Fig. 9a).

sample	j (dark) / μA cm^{-2}	**sample**	j (vis)/ μA cm^{-2}
10 Au	-2.5	10 Au	-4.7
10 Cu	-90	10 Cu	-160
5 Au/5 Cu	**-50**	5 Au/5 Cu	**-190**
5 Cu/5 Au	**-60**	5 Cu/5 Au	**-170**
TiND	-1.6	TiND	-2

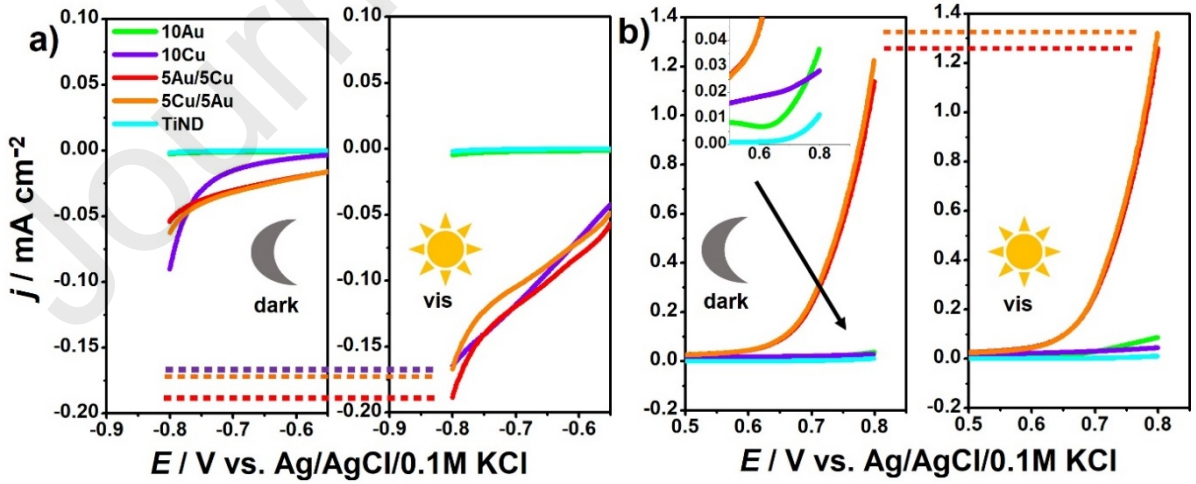

Fig. 9 The selected segments from a) cathodic and b) anodic range of linear voltammetry curves (from Fig. 7a) registered in 0.1 M NaOH in dark and under visible illumination for samples annealed at 450°C.

Regarding the LV studies carried out for the TiND electrodes annealed at 600°C, they all exhibit the resistor-like characteristics[89] (Fig.7b). Moreover, as has been already verified via linear voltammetry measurements, the differences between current densities in dark and under electrode illumination for electrodes annealed at 600°C were significantly smaller than for those kept at 450°C. Thus, once again formation of the resistive rutile titania onto the Ti substrate negatively impacts on overall electrode photoresponse.

Conclusion

In this work, we proposed formation of the Au-Cu nanomosaic onto titanium dimples via a sequential procedure covering electrochemical oxidation of Ti foil, removal of titania nanotubes layer, sputtering of thin metal layers and finally 10 min. long processing in a furnace heated up to 450°C or 600°C. The selective etching of as-grown tubular layer results in the formation of a highly ordered titanium dimpled surface acting as a hosting platform for metal nanostructures. The different temperatures of annealing and various sequence of sputtered Au and Cu metal layers had a great impact on the morphology, optical and electrochemical properties. The treatment at 450°C of titanium covered by both 5Au/5Cu or 5Cu/5Au compositions preserves the periodic system of nanocaves. However, when 600°C was applied the gold-copper nanoparticles onto the whole substrate are distributed while Ti dimples are no longer distinguished. The modulation of the optical properties is revealed as a shift in the absorbance band maximum for the bimetallic materials from ca. 470 nm towards up to ca. 900 nm with simultaneous broadening, when low and high temperature annealing was performed. The XPS

spectra recorded for Au-Cu based structure confirmed the presence of diverse Cu species, namely Au-Cu alloy, CuO, $Cu(OH)_2$. The activity of all samples was verified in 0.1 M NaOH while the electrode was maintained both in dark and when exposed to visible light, and unique faradaic processes related to the change of the gold and copper oxidation state as well as superior photoresponse of the bimetallic structures were tracked. The electrochemical behaviour of both bimetallic configurations is similar but some noticeable difference in photocurrent enhancement in favour of the 5Au/5Cu sample in both anodic and cathodic limit is observed. The synergistic effect caused by a combination of Au and Cu metals manifests as a current density almost 15 times higher than that recorded for pure gold nanostructures when the electrode is polarized at +0.8 V vs. Ag/AgCl/0.1M KCl. Summarizing, we presented the unique, combined electrochemical-thermal approach resulting in the formation of stable bimetallic mosaic structure over the nanotextured and elastic Ti foil exhibiting broad band absorbance within the visible range and boosted activity towards oxygen evolution reaction under low polarization conditions.

References

Declaration of interests

☒ The authors declare that they have no known competing financial interests or personal relationships that could have appeared to influence the work reported in this paper.

☐The authors declare the following financial interests/personal relationships which may be considered as potential competing interests:

Au-Cu nanomosaic onto titanium dimples formation via facile approach

Shift in the absorbance band maximum for the bimetallic materials from 470 nm to 900 nm

Combination of Au and Cu metals results in current density almost 15 times higher than for pure Au nanostructures

Synergistic effect between the Au and Cu can be achieved via simple thermal treatment of sputtered films

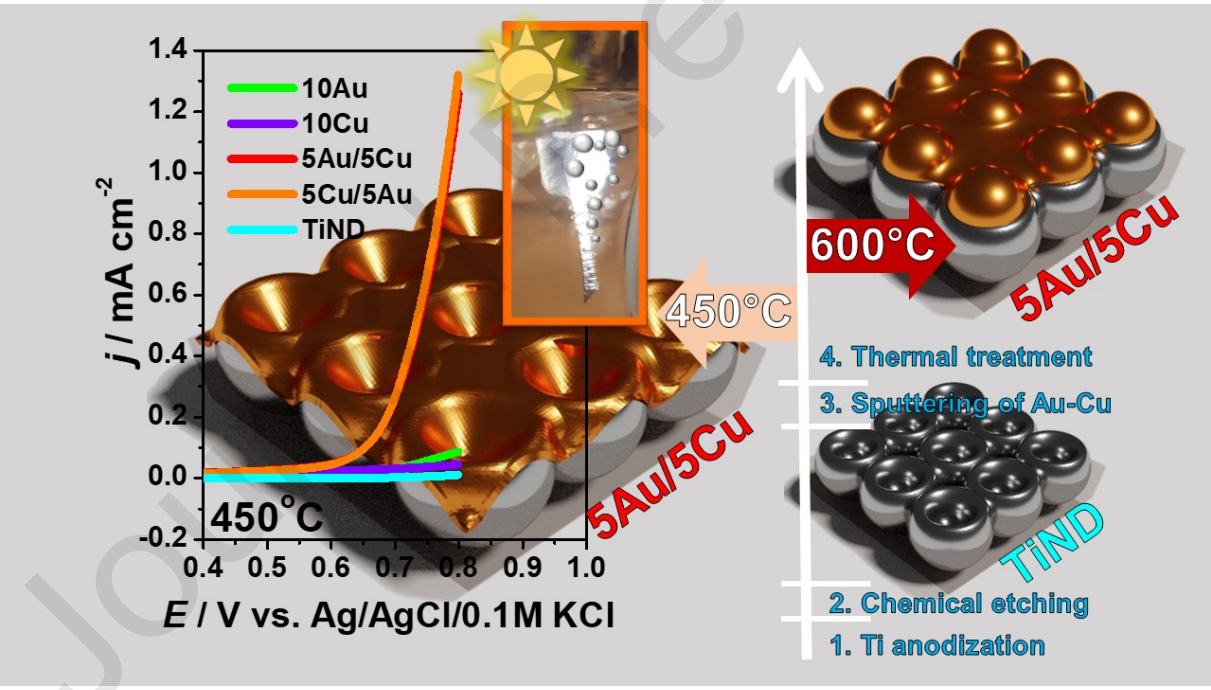

[1] C.F. Tan, A.K.S.S. Zin, Z. Chen, C.H. Liow, H.T. Phan, H.R. Tan, G.W. Ho, Inverse stellation of CuAu-ZnO multimetallic-semiconductor nanostartube for plasmon-enhanced photocatalysis, ACS Nano 12 (2018) 4512-4520. https://doi.org/10.1021/acsnano.8b00770.

[3] D.S. Lee, W. Kim, B.G. Cha, J. Kwon, S.J. Kim, M. Kim, J.H. Park, Self-position of Au NPs in perovskite solar cells: optical and electrical contribution, ACS Appl. Mater. Interfaces 8 (2016) 449-454. https://doi.org/10.1021/acsami.5b09365.13-9.

[4] S. Xu, L. Guo, Q. Sun, Z.L. Wang, Piezotronic effect enhanced plasmonic photocatalysis by AuNPs/$BaTiO_3$ heterostructures, Adv. Funct. Mater. 29 (2019) 1808737. https://doi.org/10.1002/adfm.201808737.

[5] D. Wen, W. Liu, A-K. Herrmann, D. Haubold, M. Holzschuh, F. Simon, A. Eychmüller, Simple and sensitive colorimetric detection of dopamine based on assembly of cyclodextrin-modified Au nanoparticles, Small 12 (2016) 2439-2442. https://doi.org/10.1002/smll.201503874.

[6] A. Müller, S. Peglow, M. Karnahl, A. Kruth, H. Junge, V. Brüser, C. Scheu, Morphology, optical properties and photocatalytic activity of photo- and plasma-deposited Au and Au/Ag core/shell nanoparticles on titania layers, Nanomaterials 8 (2018) 502. https://doi.org/10.3390/nano8070502.

[7] J. Ding, X. Li, L. Chen, X. Zhang, X. Tian, Photocatalytic hydrogen production over plasmonic AuCu/$CaIn_2S_4$ composites with different AuCu atomic arrangements, Appl. Catal. B 224 (2018) 322-329. https://doi.org/10.1016/j.apcatb.2017.10.045.

[8] A.L. Strickler, M. Escudero-Escribano, T.F. Jaramillo, Core–shell Au@metal-oxide nanoparticle electrocatalysts for enhanced oxygen evolution, Nano Lett. 17 (2017) 6040-6046. https://doi.org/10.1021/acs.nanolett.7b02357.

[9] L. Chen, X. Wei, X. Zhou, Z. Xie, K. Li, Q. Ruan, Z. Zheng, Large-area patterning of metal nanostructures by dip-pen nanodisplacement lithography for optical applications, Small 13 (2017) 1702003. https://doi.org/10.1002/smll.201702003.

[10] S. Chen, S.V. Jenkins, J. Tao, Y. Zhu, J. Chen, Anisotropic seeded growth of Cu–M (M = Au, Pt, or Pd) bimetallic nanorods with tunable optical and catalytic properties, J. Phys. Chem. C 117 (2013) 8924-8932. https://doi.org/10.1021/jp4013653.

[11] M. Marelli, A. Jouve, A. Villa, R. Psaro, A. Balerna, L. Prati, C. Evangelisti, Hybrid Au/CuO nanoparticles: effect of structural features for selective benzyl alcohol oxidation, J. Phys. Chem. C 123 (2019) 2864-2871. https://doi.org/10.1021/acs.jpcc.8b09449.

[12] F. Du, H. Wang, X. Jin, W. Deng, Ch. Li, Z. Ren, H. Yan, B. Yin, Selective oxidation of 1,2-propanediol to lactic acid over synergistic AuCu/TiO_2 catalysts, Catal. Lett. 149 (2019) 1037-1045. https://doi.org/10.1007/s10562-019-02670-5.

[13] S. Peiris, J. McMurtrie, H.Y. Zhu, Metal nanoparticle photocatalysts: emerging processes for green organic synthesis, Catal. Sci. Technol. 6 (2016) 320-338. https://doi.org/10.1039/C5CY02048D.

[14] Y.H. Su, W.L. Wang, Surface plasmon resonance of Au-Cu bimetallic nanoparticles predicted by a quasi-chemical model, Nanoscale Res. Lett. 8 (2013) 408. https://doi.org/10.1186/1556-276X-8-408.

[15] K. Liu, M. Ma, L. Wu, M. Valenti, D. Cardenas-Morcoso, J.P. Hofmann, J. Bisquert, S. Gimenez, W.A. Smith, Electronic effects determine the selectivity of planar Au–Cu bimetallic thin films for electrochemical CO_2 reduction, ACS Appl. Mater. Interfaces 11 (2019) 16546-16555. https://doi.org/10.1021/acsami.9b01553.

[16] B. Wang, R. Li, Z. Zhang, W. Zhang, X. Yan, X. Wu, R. Zheng, Novel Au/Cu_2O multi-shelled porous heterostructures for enhanced efficiency of photoelectrochemical water splitting, J. Mater. Chem. A 5 (2017) 14415-14421. https://doi.org/10.1039/C7TA02254A.

[17] H. Gong, W. Zhang, F. Li, R. Yang, Enhanced electrocatalytic performance of self-supported AuCuCo for oxygen reduction and evolution reactions, Electrochim. Acta 252 (2017) 261-267. https://doi.org/10.1016/j.electacta.2017.08.194.

[18] Y. Gafner, S. Gafner, L. Redel, I. Zamulin, Dual structural transition in small nanoparticles of Cu-Au alloy, J. Nanopart. Res. 20 (2018) 51. https://doi.org/10.1007/s11051-018-4161-2.

[19] P.P. Fedorov, S.N. Volkov, Au–Cu phase diagram, Rus. J. Inorg. Chem. 61 (2016) 772-775. https://doi.org/10.1134/S0036023616060061.

[20] D. Kim, C. Xie, N. Becknell, Y. Yu, M. Karamad, K. Chan, E.J. Crumlin, J.K. Norskov, P. Yang, Electrochemical activation of CO_2 through atomic ordering transformations of AuCu nanoparticles, J. Am. Chem. Soc. 139 (2017) 8329-8336. https://doi.org/10.1021/jacs.7b03516.

[21] S. Chen, Q. Sun, L. Xiao, J. Sun, Thermal stability of microstructure and mechanical properties of ultrafine-grained pure titanium, In Proceedings 2013ThermalSO

[22] W. Lipińska, K. Siuzdak, J. Ryl, P. Barski, G. Śliwiński, K. Grochowska, The optimization of enzyme immobilization at Au-Ti nanotextured platform and its impact onto the response towards glucose in neutral media, Mater. Res. Express 6 (2019) 1150e3. https://doi.org/10.1088/2053-1591/ab4fab.

[23] K. Siuzdak, D. Döhler, J. Bachmann, J. Karczewski, K. Grochowska, Light-improved glucose sensing on ordered Au-Ti heterostructure, Optik 206 (2020) 164166. https://doi.org/10.1016/j.ijleo.2019.164166.

[24] Ł. Skowroński, A.A. Wachowiak, A. Grabowski, Characterization of optical and microstructural properties of semitransparent TiO_2/Ti/glass interference decorative coatings, Appl. Surf. Sci. 388 (2016) 731-470. https://doi.org/10.1016/j.apsusc.2016.05.159.

[25] H.N. Umh, S. Yu, Y.H. Kim, S.Y. Lee, J. Yi, Tuning the structural color of a 2D photonic crystal using a bowl-like nanostructure, ACS Appl. Mater. Interfaces 8 (2016) 15802-15808. https://doi.org/10.1021/acsami.6b03717.

[26] V.V. Malkar, T. Mukherjee, S. Kapoor, Aminopolycarboxylic acids and alginate composite-mediated green synthesis of Au and Ag nanoparticles, J. Nanostruct. Chem. 5 (2015) 1-6. https://doi.org/10.1007/s40097-014-0122-1.

[27] N.A. Saad, M.H. Dar, E. Ramya, S.R.G. Naraharisetty, D. Narayana Rao, Saturable and reverse saturable absorption of a Cu_2O–Ag nanoheterostructure, J. Mater. Sci. 54 (2018) 188-199. https://doi.org/10.1007/s10853-018-2811-5.

[28] R. Li, X. Yan, L. Yu, Z. Zhang, Q. Tang, Y. Pan, The morphology dependence of cuprous oxide and its photocatalytic properties, CrystEngComm, 15 (2013) 10049-10058. https://doi.org/10.1039/C3CE41470A.

[29] A. Gołąbiewska, A. Malankowska, M. Jarek, W. Lisowski, G. Nowaczyk, S. Jurga, A. Zaleska-Medynska, The effect of gold shape and size on the properties and visible light-induced photoactivity of Au-TiO_2, Appl. Catal. B 196 (2016) 27-40. https://doi.org/10.1016/j.apcatb.2016.05.013.

[30] S. Padikkaparambil, B. Narayanan, Z. Yaakob, S. Viswanathan, S.M. Tasirin, Au/TiO_2 reusable photocatalysts for dye degradation, Int. J. Photoenergy 2013 (2013) 752605. https://doi.org/10.1155/2013/752605.

[31] S. Mohan, Y. Singh, D.K. Verma, S.H. Hasan, Synthesis of CuO nanoparticles through green route using Citrus limon juice and its application as nanosorbent for Cr(VI) remediation: process optimization with RSM and ANN-GA based model, Process Saf. Environ. 96 (2015) 156-166. https://doi.org/10.1016/j.psep.2015.05.005.

[32] H. Liu, A. Wang, Q. Sun, T. Wang, H. Zeng, Cu nanoparticles/fluorine-doped tin oxide (FTO) nanocomposites for photocatalytic H_2 evolution under visible light irradiation, Catalysts 7 (2017) 385. https://doi.org/10.3390/catal7120385.

[33] V.V. Pham, D.P. Bui, H.H. Tran, M.T. Cao, T.K. Nguyen, Y.S. Kim, V.H. Le, Photoreduction route for Cu_2O/TiO_2 nanotubes junction for enhanced photocatalytic activity, RSC Adv. 8 (2018) 12420-12427. https://doi.org/10.1039/C8RA01363B.

[34] Y-H. Chang, C-M. Wang, Y-K. Hsu, Y-H. Pai, J-Y. Lin, C-H. Lin, Graphene oxide as the passivation layer for Cu_xO photocatalyst on a plasmonic Au film and the corresponding photoluminescence study, Opt. Express 23 (2015) A1245-A1252. https://doi.org/10.1364/OE.23.0A1245.

[35] S.K. Sinha, C. Srivastava, S. Sampath, K. Chattopadhyay, Tunability of monodispersed intermetallic AuCu nanoparticles through understanding of reaction pathways, RSC Adv. 5 (2015) 4389-4395. https://doi.org/10.1039/C4RA12059K.

[36] C. Liu, H. Dong, N. Wu, Y. Cao, X. Zhang, Plasmonic resonance energy transfer enhanced photodynamic therapy with $Au@SiO_2@Cu_2O$/perfluorohexane nanocomposites, ACS Appl. Mater. Interfaces 10 (2018) 6991-7002. https://doi.org/10.1021/acsami.8b00112.

[37] M.Z. Hossain, N. Shimizu, Covalent immobilization of gold nanoparticles on graphene, J. of Phys. Chem. C 123 (2019) 3512-3516 https://doi.org/10.1021/acs.jpcc.8b09619.

[38] X. Yan, J. Sun, Y. Meng, Experimental insight into the chemical corrosion mechanism of copper with on oil-in-water emulsion solution, RSC Adv. 8 (2018) 9833-9840. https://doi.org/10.1039/C8RA00432C.

[39] H. Park, S.E. Kim, Two-step plasma treatment on copper surface for low temperature Cu thermo-compression bonding, IEEE T. Comp. Pack. Man. 10 (2020) 332-338, https://doi.org/10.1109/TCPMT.2019.2928323.

[40] Y.L. Liu, Y.C. Zhu, L.B. Qu, R. Yang, X.D. Yu, W.W. Zhao, Unique redox Reaction between CuO photocathode and cysteine: insight into the mechanism for cathodic photoelectrochemical bioanalysis, ACS Appl. Bio Mater. 2 (2019) 2703-2707. https://doi.org/10.1021/acsabm.9b00428.

[41] S. Hejazi, S. Mohajernia, Y. Wu, P. Andryskova, G. Zoppellaro, I. Hwang, O. Tomanec, R. Zboril, P. Schmuki, Intrinsic Cu nanoparticle decoration of TiO_2 nanotubes: a platform for efficient noble metal free photocatalytic H_2 production, Electrochem. Commun. 98 (2019) 82-86. https://doi.org/10.1016/j.elecom.2018.11.020.

[42] E. Völker, F.J. Williams, E.J. Calvo, T. Jacob, D.J. Schiffrin, O_2 induced Cu surface segregation in Au–Cu alloys studied by angle resolved XPS and DFT modelling, Phys. Chem. Chem. Phys. 14 (2012) 7448-7455. https://doi.org/10.1039/C2CP40565B.

[43] I. Barroso-Martín, E. Moretti, A. Talon, L. Storaro, E. Rodríguez-Castellón, A. Infantes-Molina, Au and AuCu nanoparticles supported on SBA-15 ordered mesoporous titania-silica as catalysts for methylene blue photodegradation, Materials 11 (2018) 890. https://doi.org/10.3390/ma11060890.

[44] R.J. Chimentao, F. Medina, J.L.G. Fierro, J. Llorca, J.E. Sueiras, Y. Cesteros, P. Salagre, Propene epoxidation by nitrous oxide over Au–Cu/TiO_2 alloy catalysts, J. Mol. Catal. A: Chem. 274 (2007) 159-168. https://doi.org/10.1016/j.molcata.2007.05.008.

[45] M.C. Biesinger, Advanced analysis of copper X-ray photoelectron spectra, Surf. Interface Anal. 49 (2017) 1325-1334. https://doi.org/10.1002/sia.6239.

[46] Y. Shi, Y. Zhang, X. Zhang, J. Cai, S. Lin, A non-noble metal oxide Ti_2O_3/rGO composite as efficient and highly stable electrocatalyst for oxygen reduction, Int. J. Hydrog. Energy 44 (2019) 28134-28142. https://doi.org/10.1016/j.ijhydene.2019.09.079.

[47] Y. Wang, M. Zhou, Y. He, Z. Zhou, Z. Sun, In situ loading CuO quantum dots on TiO_2 nanosheets as cocatalyst for improved photocatalytic water splitting, J. Alloys Compd. 813 (2019) 152184. https://doi.org/10.1016/j.jallcom.2019.152184.

[48] A. Mezni, M.M. Ibrahim, M. El-Kemary, A.A. Shaltout, N.Y. Mostafa, J. Ryl, T. Kumeria, T. Altalhi, M.A. Amin, Cathodically activated Au/TiO_2 nanocomposite synthesized by a new facile solvothermal method: An efficient electrocatalyst with Pt-like activity for hydrogen

generation, Electrochim. Acta 290 (2018) 404-418. https://doi.org/10.1016/j.electacta.2018.08.083.

[49] K. Grochowska, J. Ryl, J. Karczewski, G. Śliwiński, A. Cenian, K. Siuzdak, Non-enzymatic flexible glucose sensing platform based on nanostructured TiO_2 – Au composite, J. Electroanal. Chem. 837 (2019) 230-239. https://doi.org/10.1016/j.jelechem.2019.02.040.

[50] N. Shen, H. Xu, W. Zhao, Y. Zhao, X. Zhang, Highly responsive and ultrasensitive non-enzymatic electrochemical glucose sensor based on Au foam, Sensors 19 (2019) 1203. https://doi.org/10.3390/s19051203.

[51] Y. He, G. Wei, J. Lin, M. Sun, Z. Li, Cu and Ni nanoparticles deposited on ITO electrode for nonenzymatic electrochemical carbohydrates sensor applications, Electroanalysis 29 (2017) 965-974. https://doi.org/10.1002/elan.201600606.

[52] L. Zhang, C. Ye, X. Li, Y. Ding, H. Liang, G. Zhao, Y. Wang, A CuNi/C nanosheet array based on a metal–organic framework derivate as a supersensitive non-enzymatic glucose sensor, Nano-Micro Lett. 10 (2018) 28. https://doi.org/10.1007/s40820-017-0178-9.

[53] C. Lu, Z. Li, L. Ren, N. Su, D. Lu, Z. Liu, In situ oxidation of Cu_2O crystal for electrochemical detection of glucose, Sensors 19 (2019) 2926. https://doi.org/10.3390/s19132926.

[54] T. Pasini, M. Piccinini, M. Blosi, R. Bonelli, S. Albonetti, N. Dimitratos, J.A. Lopez-Sanchez, M. Sankar, Q. He, C.J. Kiely, G.J. Hutchings, F. Cavani, Selective oxidation of 5-hydroxymethyl-2-furfural using supported gold–copper nanoparticles, Green Chem. 13 (2011) 2091-2099. https://doi.org/10.1039/C1GC15355B.

[55] S.D. Giri, A. Sarkar, Electrochemical study of bulk and monolayer copper in alkaline solution, J. Electrochem. Soc. 163 (2016) H252. https://doi.org/10.1149/2.0071605jes.

[56] X. Zhang, A. Shan, S. Duan, H. Zhao, R. Wang, W. M. Lau, Au@Co_2P core/shell nanoparticles as a nano-electrocatalyst for enhancing the oxygen evolution reaction, RSC Adv. 9 (2019) 40811-40818. https://doi.org/10.1039/C9RA07535F.

[57] J. Pei, J. Mao, X. Liang, C. Chen, Q. Peng, D. Wang, Y. Li, Ir–Cu nanoframes: one-pot synthesis and efficient electrocatalysts for oxygen evolution reaction, Chem. Commun. 52 (2016) 3793-3796. https://doi.org/10.1039/C6CC00552G.

[58] H. Gong, S. Lu, P. Strasser, R. Yang, Highly efficient AuNi-Cu_2O electrocatalysts for the oxygen reduction and evolution reactions: Important role of interaction between Au and Ni engineered by leaching of Cu_2O, Electrochim. Acta 283 (2018) 1411-1417. https://doi.org/10.1016/j.electacta.2018.07.083.

[59] H. Chen, M. Nishijima, G. Wang, S. Khene, M. Zhu, X. Deng, X. Zhang, W. Wen, Y Luo, Q. He, The ordered and disordered nano-intermetallic AuCu/C catalysts for the oxygen reduction reaction: The differences of the electrochemical performance, J. Electrochem. Soc. 164 (2017) F1654. https://doi.org/10.1149/2.1331714jes.

[60] G. Wang, L. Xiao, B. Huang, Z. Ren, X. Tang, L. Zhuang, J. Lu, AuCu intermetallic nanoparticles: surfactant-free synthesis and novel electrochemistry, J. Mater. Chem. 22 (2012) 15769-15774. https://doi.org/10.1039/C2JM32264A.

[61] L.D. Burke, J.M. Moran, P.F. Nugent, Cyclic voltammetry responses of metastable gold electrodes in aqueous media, J. Solid State Electrochem. 7 (2003) 529-538. https://doi.org/10.1007/s10008-003-0359-y.

[62] J. Grotberg, A. Hamlekhan, A. Butt, S. Patel, D. Royhman, T. Shokuhfar, C. Sukotjo, C. Takoudis, M.T. Mathew, Thermally oxidized titania nanotubes enhance the corrosion resistance of Ti6Al4V, Mater. Sci. Eng. C 59 (2016) 677-689. https://doi.org/10.1016/j.msec.2015.10.056.

[63] K. U. Savitha, H. Gurumallesh Prabu, One-pot synthesis of PANI–TiO_2 (anatase) hybrid of low electrical resistance using $TiCl_4$ as precursor, Mater. Chem. Phys. 130 (2011) 275-279. https://doi.org/10.1016/j.matchemphys.2011.06.037.

[64] M. Łukaszewski, M. Soszko, A. Czerwiński, Electrochemical methods of real surface area determination of noble metal electrodes – an overview, Int. J. Electrochem. Sci. 11 (2016) 4442-4469. https://doi.org/10.20964/2016.06.71.

[65] N. Mayet, K. Servat, K.B. Kokoh, T.W. Napporn, Probing the surface of noble metals electrochemically by underpotential deposition of transition metals, Surfaces 2 (2019) 257-276. https://doi.org/10.3390/surfaces2020020.

[66] F. Finger, K. Welter, F. Urbain, V. Smirnov, B. Kaiser, W. Jaegermann, Photoelectrochemical water splitting using adapted silicon based multi-junction solar cell structures: Development of solar cells and catalysts, upscaling of combined photovoltaic-electrochemical devices and performance stability, Z. Phys. Chem. (2019). https://doi.org/10.1515/zpch-2019-1453.

[67] S. Jia, X. Li, B. Zhang, J. Yang, S. Zhang, S. Li, Z. Zhang, TiO_2/CuS heterostructure nanowire array photoanodes toward water oxidation: The role of CuS, Appl. Surf. Sci. 463 (2019) 829-837. https://doi.org/10.1016/j.apsusc.2018.09.003.

[68] M. Morozova, P. Kluson, J. Krysa, P. Dzik, M. Vesely, O. Solcova, Thin TiO_2 films prepared by inkjet printing of the reverse micelles sol–gel composition, Sens. Actuators B Chem. 160 (2011) 371-378. https://doi.org/10.1016/j.snb.2011.07.063.

[69] H. Krysova, M. Zlamalova, H. Tarabkova, J. Jirkovsky, O. Frank, M. Kohout, L. Kavan, Rutile TiO_2 thin film electrodes with excellent blocking function and optical transparency, Electrochim. Acta 321 (2019) 134685. https://doi.org/10.1016/j.electacta.2019.134685.

[70] S.M. Pawar, B.S. Pawar, B. Hou, J. Kim, A.T. Aqueel Ahmed, H.S. Chavan, Y. Jo, S. Cho, A.I. Inamdar, J.L. Gunjakar, H. Kim, SN. Cha, H. Im, Self-assembled two-dimensional copper oxide nanosheet bundles as an efficient oxygen evolution reaction (OER) electrocatalyst for water splitting applications J. Mater. Chem. A 5 (2017) 12747-12751. https://doi.org/10.1039/C7TA02835K.

[71] S.Z. Oener, S.A. Mann, B. Sciacca, C. Sfiligoj, J. Hoang, E.C. Garnett, Au-Cu_2O core-shell nanowire photovoltaics, Appl. Phys. Lett. 106 (2015) 023501. https://doi.org/10.1063/1.4905652.

[72] S.Y. Tee, E. Ye, P.H. Pan, C.J. J. Lee, H.K. Hui, S.Y. Zhang, L. D. Koh, Z. Dong, M.Y. Han, Fabrication of bimetallic Cu/Au nanotubes and their sensitive, selective, reproducible and reusable electrochemical sensing of glucose, Nanoscale 7 (2015) 11190-11198. https://doi.org/10.1039/C5NR02399H.

[73] Y. Tang, Q. Liu, X. Liu, X. Yang, M. Wei, M. Zhnag, Copper oxide coated gold Nanorods like a film: A facile route to nanocomposites for electrochemical application, J. Electroanal. Chem. 806 (2017) 814. https://doi.org/10.1016/j.jelechem.2017.10.032.

[74] A.S. Rajpurohit, N.S. Punde, A.K. Srivastava, An electrochemical sensor with a copper oxide/gold nanoparticle-modified electrode for thesimultaneous detection of the potential diabeticbiomarkers methylglyoxal and its detoxificationenzyme glyoxalase, New J. Chem. 43 (2019) 16572-16582. https://doi.org/10.1039/C9NJ03553B.

[75] I. Nadjovski, PR. Selvakannan, S.K. Bhargava, A.P. O'Mullane, Formation of nanostructured porous Cu–Au surfaces: the influence of cationic sites on (electro)-catalysis, Nanoscale 4 (2012) 6298-6306. https://doi.org/10.1039/C2NR31409F.

[76] R.A. Ismail, R.S. Abdul-Hamed, Laser ablation of Au–CuO core–shell nanocomposite in water for optoelectronic devices, Mater. Res. Express 4 (2017) 125020. https://doi.org/10.1088/2053-1591/aa9e14.

[77] A.B. Ghosh, N. Saha, A. Sarkar, A.K. Dutta, S.K. Maji, B. Adhikary, Observation of enhanced photocurrent response in M–$CuInS_2$ (M = Au, Ag) heteronanostructures: phase selective synthesis and application, New J. Chem. 41 (2017) 692-701. https://doi.org/10.1039/C6NJ02439D.

[78] J.S. Yoon, J.W. Lee, Y.M. Sung, Enhanced photoelectrochemical properties of Z-scheme ZnO/p-n Cu_2O PV-PEC cells, J. Alloys Compd. 771 (2019) 869-876. https://doi.org/10.1016/j.jallcom.2018.09.021.

[79] L.J. Minggu, K.H. Ng, H.A. Kadir, M. Bin Kassim, Bilayer n-WO_3/p-Cu_2O photoelectrode with photocurrent enhancement in aqueous electrolyte photoelectrochemical reaction, Ceramic Intern. 40 (2014) 16015-16021. https://doi.org/10.1016/j.ceramint.2014.07.135.

[80] L. Liu, X. Gu, C. Sun, H. Li, Y. Deng, F. Gao, L. Dong, In situ loading of ultra-small Cu_2O particles on TiO_2nanosheets to enhance the visible-light photoactivity, Nanoscale 4 (2012) 6351-6359. https://doi.org/10.1039/C2NR31859H.

[81] Y. Sugano, Y. Shiraishi, D. Tsukamoto, S. Ichikawa, S. Tanaka, T. Hirai, Supported Au–Cu bimetallic alloy nanoparticles: an aerobic oxidation catalyst with regenerable activity by visible-light irradiation, Angew. Chem. 125 (2013) 5403-5407. https://doi.org/10.1002/ange.201301669.

[82] M. Liu, W. Zhou, T. Wang, D. Wang, L. Liu, J. Ye, High performance Au-Cu alloy for enhanced visible-light water splitting driven by coinage metals, Chem. Commun. 52 (2016) 4694-4697. https://doi.org/10.1039/C6CC00717A.

[83] B. Kumar, S. Saha, M. Basu, A.K. Ganguli, Enhanced hydrogen/oxygen evolution and stability of nanocrystalline (4–6 nm) copper particles, J. Mater. Chem. A 1 (2013) 4728-4735. https://doi.org/10.1039/C3TA01194A.

[84] H. Yoo, S. Kahng, K.J. Hyeun, Z-scheme assisted ZnO/Cu_2O-CuO photocatalysts to increase photoactive electrons in hydrogen evolution by water splitting, Sol. Energy Mater. Sol. Cells 204 (2020) 110211. https://doi.org/10.1016/j.solmat.2019.110211.

[85] H. Hou, M. Shang, F. Gao, L. Wang, Q. Liu, J. Zheng, Z. Yang, W. Yang, Highly efficient photocatalytic hydrogen evolution in ternary hybrid TiO_2/CuO/Cu thoroughly mesoporous

nanofibers ACS Appl. Mater. Interfaces 8 (2016) 20128-20137. https://doi.org/10.1021/acsami.6b06644.

[86] D. Zeng, L. Yang, P. Zhou, D. Hu, Y. Xie, S. Li, L. Jiang, Y. Ling, J. Zhao, Au-Cu alloys deposited on titanium dioxide nanosheets for efficient photocatalytic hydrogen evolution, Int. J. Hydrog. Energy 43 (2018) 15155-15163. https://doi.org/10.1016/j.ijhydene.2018.06.078.

[87] S. Fu, J. Chen, H. Han, W. Wang, H. Shi, J. Fu, Y. Jia, ZnO@Au@Cu_2O nanotube arrays as efficient visible-light-driven photoelectrod, J. Alloys Compd. 799 (2019) 183-192. https://doi.org/10.1016/j.jallcom.2019.05.340.

[88] J. Xue, D. Jing, H. Xie, W. Ni, X. Li, Exponential dependence of photocatalytic activity on linker chain length of Au-linker-Cu_2O plasmonic photocatalysts with sub-nanometer precision, Catal. Lett. 148 (2018) 363-3369. https://doi.org/10.1007/s10562-018-2560-8.

[89] A.J. Bard, L.R. Faulkner, Electrochemical Methods, Fundamentals and Applications, Second edition, Department of Chemistry and Biochemistry University of Texas at Austin, John Wiley & Sons, 2001.